Slowdown of Shirase Glacier, East Antarctica, caused by strengthening alongshore winds

Bertie W.J. Miles*[1,2], Chris R. Stokes[2], Adrian Jenkins[3], Jim .R. Jordan[3,4], Stewart .S.R. Jamieson[2], G. Hilmar. Gudmundsson[3]

[1]School of Geosciences, Edinburgh University, Edinburgh, EH8 9XP, UK

[2]Department of Geography, Durham University, Durham, DH1 3LE, UK

[3]Department of Geography and Environmental Sciences, Northumbria University, Newcastle upon Tyne, NE1 8ST, UK

[4]Laboratoire de Glaciologie, Université Libre de Bruxelles, Brussels, Belgium

*Correspondence to Bertie.Miles@ed.ac.uk

Abstract

Around large parts of West Antarctica and in Wilkes Land, East Antarctica, increased wind-forced intrusions of modified Circumpolar Deep Water (mCDW) onto the continental shelf have been associated with mass loss over the last few decades. Observations have also confirmed relatively high basal melt rates of up to 16 m a^{-1} underneath the Shirase ice tongue in Enderby Land, East Antarctica. These high basal melt rates are also caused by intrusions of mCDW onto the continental shelf, but the catchment of Shirase Glacier has been gaining mass, a trend often attributed to increased precipitation. Here, we document the dynamical ocean-driven slowdown, ice surface thickening and grounding line advance of Shirase Glacier, in response to strengthening easterly winds that reduce mCDW inflow and decrease basal melt rates. Our findings are significant because they demonstrate that warm ice shelf cavity regimes are not universally associated with glacier acceleration and mass loss in Antarctica, and they highlight the overlooked role of the impact of easterly winds in the recent mass gain of the Shirase Glacier catchment.

1. Introduction

Shirase Glacier is one of the fastest flowing outlet glaciers in East Antarctica, reaching speeds in excess of 2,200 m a^{-1} across its grounding line, before flowing into Lützow-Holm Bay (Fig. 1). Its

annual ice discharge approaches 15 Gt a^{-1} (Rignot et al., 2019) and it drains a catchment containing 1.2 m of sea level equivalent (Fig.1, Morlighem et al., 2020). This rapid ice flow speed is associated with vigorous melt underneath its floating tongue, where basal melt rates were observed to vary over the course of the year between 7 and 16 m a^{-1} in 2018, 16 km downstream of the glacier's grounding line (Hirano et al., 2020). These high melt rates are caused by warm modified Circumpolar Deep Water (mCDW) intruding onto the continental shelf and being transported directly to the glacier via bathymetric troughs (Fig. 1; Moriwaki & Yoshida, 1983; Hirano et al., 2020), a process referred to as Mode 2 melting (Jacobs et al., 1992). Elsewhere in Antarctica, most regions that experience this mode of oceanic melt have been losing mass e.g. the Amundsen Sea (Jenkins et al., 2018; Mouginot et al., 2014), the Western Antarctic Peninsula (Cook et al., 2016) and Wilkes Land (Rintoul et al., 2016; Greene et al., 2017; Stokes et al., 2022); and hinting that intrusions of mCDW have become more potent over recent decades in these locations. However, mass loss has not been observed in the Shirase Glacier catchment and, between 2003 and 2019, its drainage basin (sometimes referred to as drainage basin 7 in Antarctic-wide studies (e.g. Smith et al., 2020) gained mass at a rate of $+25 \pm 6$ Gt a^{-1}, which is the largest magnitude of imbalance of all drainage basins in East Antarctica (Smith et al., 2020), including the comparatively well studied drainage basin 13 in Wilkes Land (-20 ± 14 Gt a^{-1}).

The mass gain and thickening in the Shirase catchment over the past two decades (Schröder et al., 2019; Smith et al., 2020) has been hypothesized to have been caused by increased precipitation across the wider Dronning Maud and Enderby Land regions (Smith et al., 2020). Prior to this, however, earlier field-based estimates, using repeat triangulation surveys in 1969 and 1973, demonstrated ice surface lowering of around 0.7 m a^{-1} around 100-200 km inland of the Shirase Glacier grounding line (Mae & Naruse, 1978; Naruse, 1979; Nishio et al., 1989). Furthermore, repeat GPS surveys in 1980 and 1988 revealed a thinning rate of around 0.5 m a^{-1} around 100-150 km inland of the grounding line (Toh et al., 1992). These rates of surface lowering during that time are comparable with some of the fastest rates of thinning observed across Antarctica over the past decade and occurred at similar distances inland of the grounding line (Smith et al., 2020). Moreover, this surface lowering in the 1970s and 1980s may have been part of a much longer-term signal with ice core records estimating a surface lowering of 350 m over the past 2000 years of the Mizuho Plateau (Kameda et al., 1990), which is located around 200 km inland of the Shirase coastline. The surface lowering over the past 2000 years is also coincident with an increase in ice discharge from the Lützow-Holm Bay, which has been estimated from subglacial erosion rates (Sproson et al., 2021).

Oceanographic observations in Lützow-Holm Bay in 2018 have revealed a two-layered structure with a cool and relatively fresh layer of Winter Water overlying a warm and saline layer of mCDW, where

temperatures near the ice front seasonally exceed the *in situ* melting point by 2.7 °C (Hirano et al., 2020). Observations and modelling demonstrate a strong seasonal variation in the basal melt rate of the Shirase ice tongue (Hirano et al., 2020; Kusahara et al., 2021), which is caused by seasonal variations in the depth of the thermocline forced by the strength of the alongshore easterly winds near the continental shelf (Ohshima et al., 1996). To date, there is no evidence of large seasonal variations in ice flow speed at the grounding line, but observations show some seasonal variation in ice flow speed on the floating tongue that could be connected to external forcing (Nakamura et al., 2007; 2010).

There have been several studies analysing the ice flow dynamics of the Shirase Glacier, largely covering short sub-decadal time periods (Pattyn & Derauw, 2002; Pattyn & Naruse, 2003; Nakamura et al., 2010; Aoyama et al., 2013). However, the longer-term geological signal of ice sheet thinning and increased ice discharge (Sproson et al., 2021), along with observations of thinning in the 1970s and 1980s (Mae & Naruse, 1978; Naruse, 1979; Nishio et al., 1989; Toh et al., 1992), followed by thickening from the 2000s (Schröder et al., 2019; Smith et al., 2020) raise some important questions into the processes causing this switch from mass loss to mass gain. In this study, we produce a time series of ice flow speed that spans 47 years and show that long-term ice speed trends coincide with alongshore wind speeds and their impact on intrusions of mCDW. We then discuss how these observations may relate to wider hemispheric trends in atmospheric circulation and what this may mean for the future mass balance of the Shirase catchment and the wider Dronning Maud and Enderby Land sectors.

2. Data and Methods

2.1 Ice-front position, ice speed, grounding line and ice thickness

We create a time series of ice-front positions between 1963 and 2020 using a variety of different sources including: ARGON imagery from 1963, Landsat-1 imagery from 1973, Landsat-5 imagery from 1984, Landsat-4 imagery from 1988, RADARSAT RAMP mosaic from 1997 (Jezek et al., 2013), and MODIS imagery from 2000-2020, with the spatial resolution of the satellite data ranging from 15-250 m. In each case, we map the outer limit of the collection of loosely bound icebergs that form the Shirase ice tongue that are typically surrounded by a smoother surface of fast ice (Fig. 1 & 2a). Errors associated with this mapping are insignificant in the context of the ice tongue typically advancing 2,500 m a^{-1}, or retreating in short-lived calving events typically greater than 10 km.

We calculate 18 ice speed estimates for Shirase Glacier between 1973 and 2020. For 1973 we use a pair of Landsat-1 (band 7) images from the 25th January 1973 and the 21st January 1974 that we manually co-register to each other, before co-registering to a Landsat-8 image. The combination of the relatively coarse Landsat-1 imagery (60 m) and the development of surface melt ponding over the fast-flowing section of the glaciers between the two images prevented the automatic extraction of ice speed. Instead, we extract an ice speed estimate by manually tracking the displacement of a prominent rift ~24 km downstream of the grounding line (Fig. 2c). Errors associated with the manual tracking of this rift stem from the co-registration between the two image pairs which we estimate to be one
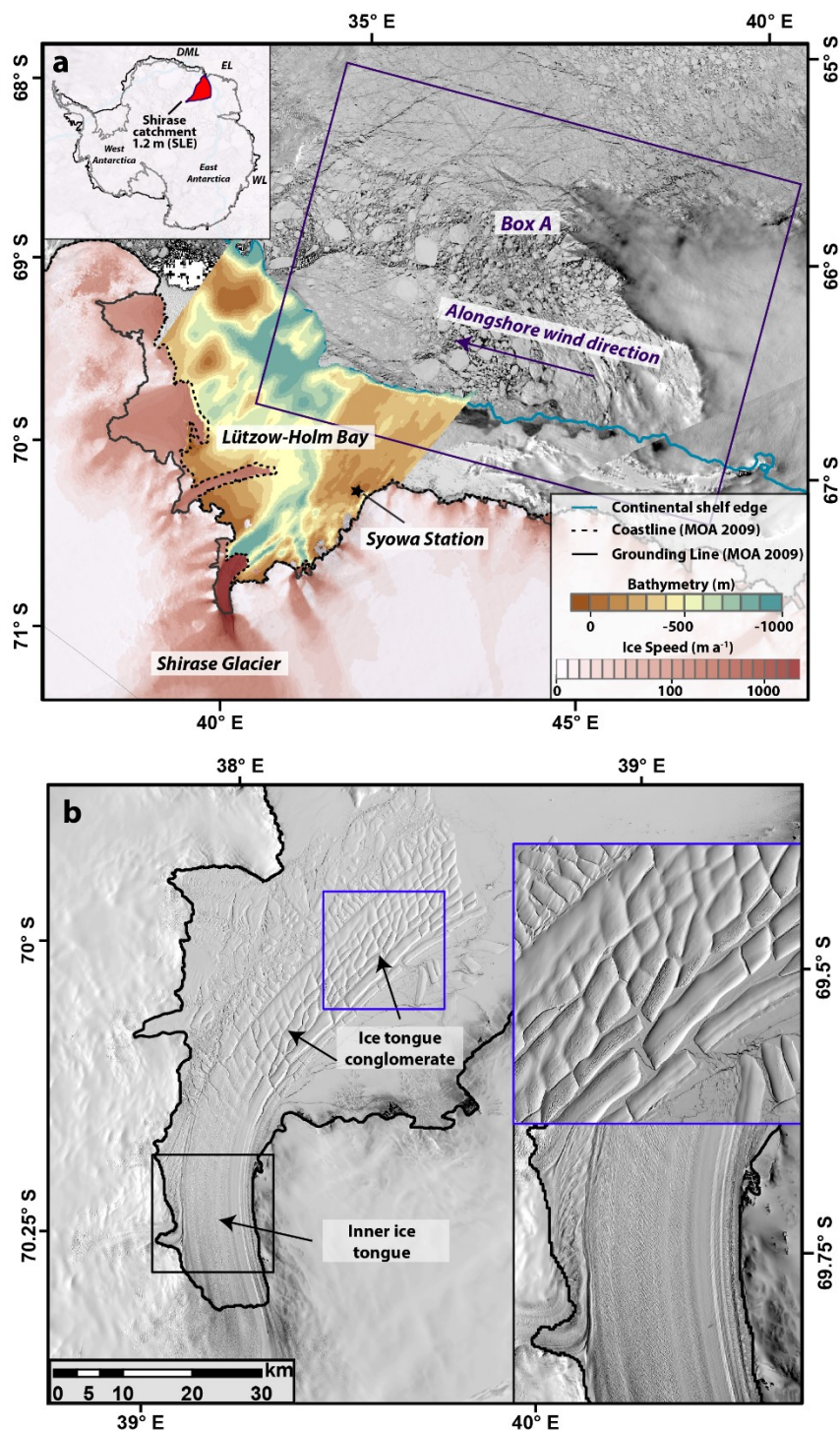
Figure 1: a) MODIS image of Lützow-Holm Bay and Shirase Glacier from the 4th November 2019 obtained from NASA WorldView. Overlain is the ITS_LIVE composite velocity product in logarithmic scale (Gardner et al., 2018; 2020), 1000 m bathymetric contour obtained from BedMachine (Morlighem et al., 2020) which is taken as the continental shelf boundary and bathymetry of the Lützow-Holm Bay (Kusahara et al., 2021). Note the deep trough connecting Shirase Glacier to the open ocean. The location of the Syowa research station and Box A, the region where ERA5 derived winds were extracted are also shown. The initials in the inset refer to the following, DML (Dronning Maud Land), EL (Enderby Land), WL (Wilkes Land). **b)** Landsat 8 image from November 2020 showing the structure of the Shirase ice tongue. The blue box is a zoomed in section of the ice tongue conglomerate that is unconstrained. The black box is a zoomed in section of the inner section of the ice tongue that is constrained by fjord walls on either side. The black line on both images is the MODIS 2009 grounding line and coastline (Scambos et al., 2007; Harran et al., 2019). Landsat images are courtesy of the U.S. Geological Survey.

pixel (60 m; Animation S1). For 1988, we use a pair of Landsat-4 (band 3) images from the 14th January 1988 and the 15th February 1988 that we also co-register to a Landsat-8 image. The quality of the Landsat-5 images (30 m resolution) is superior to that of the Landsat-1 imagery and, in the absence of significant surface melt ponding, we use the feature tracking software COSI-CORR (Leprince et al., 2007; Scherler et al., 2008) to extract ice speed. For these images, co-registration error is negligible (Animation S2) and error in the feature tracking is estimated at <0.5 pixels (e.g. Heid and Kääb, 2012). Because of the close time separation of the image pairs this results in a larger error of ± 171 m a^{-1}.

For 2000-2018 we use 14 annual ice speed mosaics from the ITS_LIVE dataset which cover Shirase Glacier (Gardner et al., 2018) and use the corresponding error grids for error values, which range from ± 1 to ± 32 m a^{-1}. For 2019 (n = 27) and 2020 (n = 19) we take an average of all GoLIVE generated ice speed fields (Fahnestock et al., 2016; Scambos et al., 2016) with a time separation of 16-320 days from scene ID's 149_109 and 150_109. Taking an average of multiple ice speed grids reduces error and, as such, we prescribe a nominal error of 16 m a^{-1}, based on the average value from the ITS_LIVE mosaics. We extract ice speed profiles from each time period across a transect, T1 (Fig. 2a), and also produce a time-series of ice speed change where T1 crosses the grounding line. In 1973, the only possible observation of ice speed was extracted 24 km downstream of the grounding line (Point x; Fig. 2a) and there are no observations directly at the grounding line. To account for this, we estimate ice speed at the grounding line in 1973 using the average difference between point x, 24 km downstream of the grounding line, and where T1 crosses the grounding line in each of the other 17 ice speed profiles (1988-2020). Across these profiles, ice speed was on average 2% slower (ranging from 1% to 4%) at the grounding line, compared to ice speed at point x. Therefore, to estimate ice speed at the grounding line in 1973 we reduce the ice speed observed 24 km downstream of the

141   grounding line by 2 ±1%. We also include the measurements of ice speed from Nakamura et al. (2007)

142   at the grounding line derived from the JERS-1 satellite in 1996, 1997 and 1998.

143   To estimate the direction and magnitude of any migration in the Shirase Glacier grounding line we

144   compare time stamped digital elevation model (DEM) strips with a spatial resolution of 2 m from the

145   6th January 2013 and the 8th October 2015 from the REMA project (Howat et al., 2019). We select

146   these strips because they cover the complete Shirase Glacier grounding line and represent the longest

147   time gap in the record. This is in addition to a SPOT5-HRS DEM from the SPIRIT project (Korona

148   et al., 2009) from the 8th February 2008, with a spatial resolution of 40 m. Elevation uncertainty is

149   estimated at around 4 m by comparing derived elevations from exposed bedrock between the two

150   REMA DEM's and a larger uncertainty of around 7 m between the SPOT5-HRS and REMA DEM's.

151   The tidal amplitude of the region is limited to 0.2 m (Aoki et al., 2000) and is deemed insignificant.

152   We extract elevation profiles along transect T1 (Fig. 2a) from these dates. A comparison of elevation

153   profiles cannot provide a location of the true grounding line position, but any horizontal migration of

154   these elevation slopes can provide reasonable estimates in both the direction and rate of grounding

155   line migration (Fricker et al., 2009; Brunt et al., 2010).

156   We also extract an ice thickness change time-series from the dataset presented in Schröder et al.

157   (2019) from point IT, which is around 20 km inland of the grounding line (Fig. 2a). This multi-

158   mission dataset spans between 1978 and 2017 and contains data from a variety of satellites. We use

159   the accompanying uncertainty estimates described in Schröder et al. (2019). We also utilize modelled

160   basal melt rate anomalies of the Shirase ice tongue that are derived by an ocean model that is forced

161   by ERA-Interim wind reanalysis between 2008 and 2018 by Kusahara et al. (2021). The basal melt

162   rate dataset contains melt anomalies that have been simulated with fast ice cover and a hypothetical

163   no fast ice scenario (see Fig. 20; Kusahara et al., 2021). We use the melt rates with fast ice cover

164   because persistent fast ice cover remained throughout our observational period, aside from a few

165   sporadic partial breakouts in the summer months.

166

2.2 Climatological data

167

168   We extract mean monthly ERA5 (Hersbach et al., 2020) 10 m zonal (U) and meridional winds (V)

169   speeds with a gridded 30 km spatial resolution between 1979 and 2021 from a box approximately

170   340 x 250 km adjacent to the coastline (Box A; Fig. 1a). We do not extend the box all the way into

171   Lützow-Holm Bay because it is semi-permanently covered with landfast sea-ice (Fig. S1) that

172   dampens the impact of winds on ocean circulation. We then calculate alongshore easterly wind speed

173   using an alongshore angle of 80° from due north:

$$A = W \cos(\theta - 80)$$

Where W is wind speed and θ is wind direction. Using the ERA5 data, we also calculate the linear trend in zonal wind between 1979 and 2021 across a wider region of the Dronning Maud and Enderby Land coastlines. We also extract a precipitation time series across Shirase Glacier using the regional climate model MAR between 1979 and 2019 (Kittel et al., 2021).

3. Results

We observe a total range of nearly 90 km in the ice-front position of the Shirase ice tongue between 1963 and 2020 (Fig. 2b). Its maximum length was in 1963, before retreating to its minimum extent in 1988 (Fig. 2a, b). Since 1988 there has been a general pattern of advance with a few sporadic calving events (Fig. 2a, b). Most of the variation in the extent of the Shirase ice tongue is in the heavily fractured and unconstrained ice tongue conglomerate (Fig. 1b; Fig. 2a). The only exception to this was in 1988 when the ice tongue retreated to the entrance of the narrow and more constrained section of its fjord, 24 km advanced of its 2009 grounding line (Fig. 2a).

188
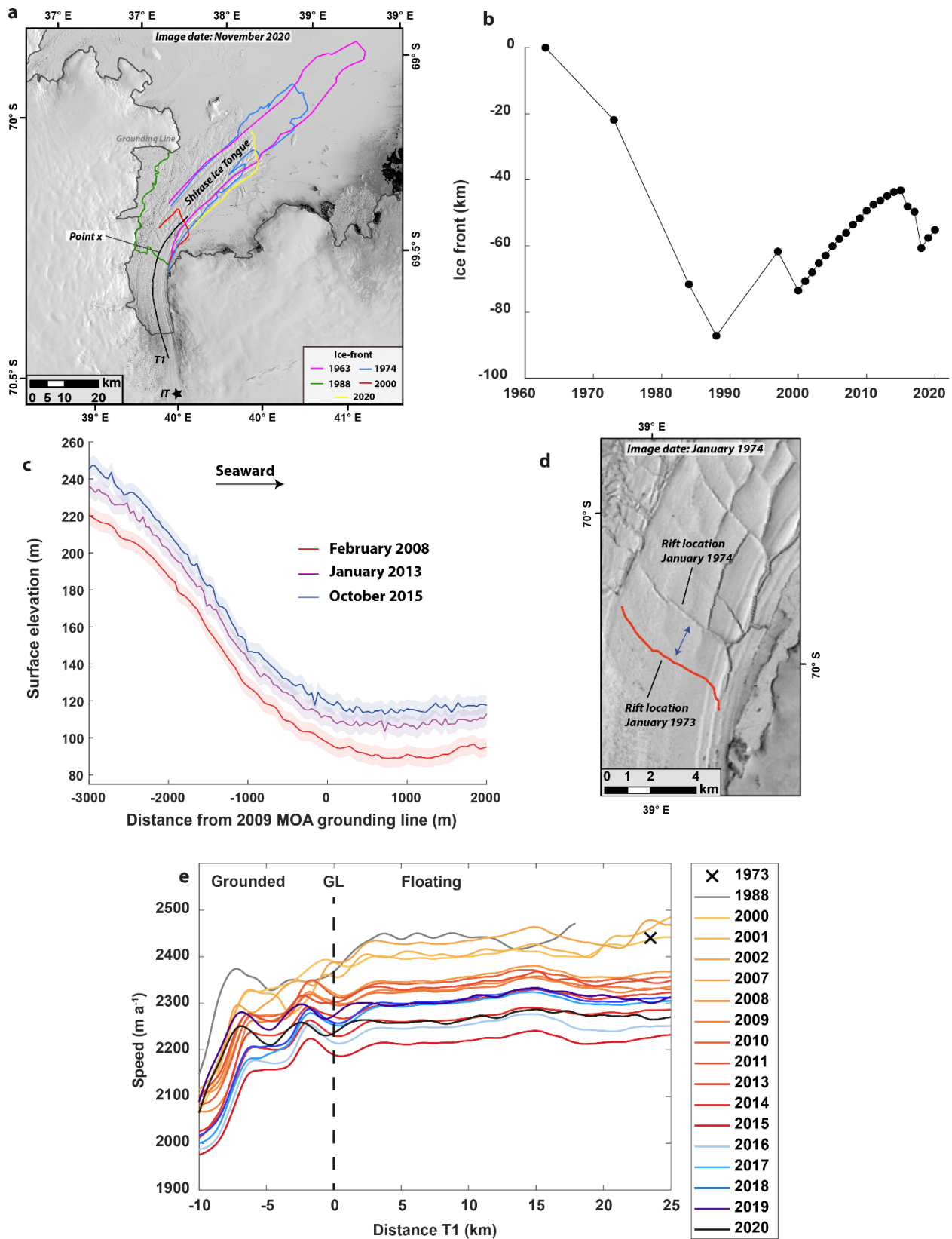
Figure 2: a) Landsat-8 image from November 2020 showing the Shirase ice tongue. Overlain are selected ice-front positions from 1963, 1974, 1988, 2000 and 2020; along with the transect, T1, used to extract ice speed profiles and point x, which is the location of the 1973/74 ice speed estimate on the floating tongue. Point IT is the location of the ice thickness time-series. The grey line is the MODIS 2009 grounding line (Scambos et al., 2007, Harran et al., 2021). **b)** Change in ice-front extent

relative to 1963. **c)** Surface elevation profiles along a small section of T1 as it intersects the grounding line from February 2008, January 2013 and October 2015 showing a seaward migration of the surface slope **d)** Landsat-1 image showing the rift used to estimate ice speed in 1973/74. The red line is the digitized rift from January 1973. **e)** Ice speed profiles from transect T1 between 1973 and 2020. The black cross represents the ice speed measurement from 1973/74. Landsat images are courtesy of the U.S. Geological Survey.

Ice speed profiles along the transect (T1, Fig. 2a) show a uniform pattern of change across both the grounded and floating sections of Shirase Glacier (Fig. 2e). At the grounding line, we observe little change in ice speed between 1973 and 1988, although we note the larger uncertainty in the 1988 estimate of ±171 m a^{-1} (Fig. 3b) and we cannot rule out interannual variations in ice speed within this date range. Between 1988 and 1996 we observe a $2 \pm7\%$ slowdown and a $2 \pm1\%$ increase in ice speed between 1997 and 2000 (Fig. 3a). Post-2000 we observe a slowdown, with an $8 \pm1\%$ decrease in ice speed between 2000 and 2015 (Fig. 3b). Between 2015 and 2019 ice speed increased by $4 \pm1\%$ (Fig. 3a). Elevation profiles along a section of T1 in 2008, 2013 and 2015 show a seaward migration of the surface slope as it approaches the grounding line (Fig. 2d), which is indicative of grounding line advance and can be visualised in animation S3. Between February 2008 and October 2015 we estimate that the grounding line advanced around 400 m (~50 m yr^{-1}) from measuring the seaward displacement of the surface slope, an estimate that is broadly consistent with CryoSat based observations of seaward grounding line migration between 2010 and 2016 (~30 m a^{-1}; Konrad et al., 2018). Observations of ice thickness change 20 km inland of the grounding line show a thinning trend of 0.27 ± 0.33 m a^{-1} between 1987 and 1997, before reversing to a thickening trend of 0.19 ± 0.10 m a^{-1} between 1997 and 2017 (Fig. 3b).

ERA5 derived estimates of alongshore easterly wind speed between 1979 and 2020 show limited variation between 1984 and the early 1990s (Fig. 3a). In the early 1990s there was a small increase in alongshore wind speed, before a more marked increase from 2000-2010 where alongshore wind speed increased from around 4 m s^{-1} to 4.8 m s^{-1} (Fig. 3a). This is before falling slightly to around 4.5 m s^{-1} between 2010 and 2018, which is coincident with an increase in basal melt rate anomalies (Fig. 3a). The multidecadal trend in zonal wind shows a trend for a strengthening of wind in an easterly direction at the continental shelf boundary over much of Enderby Land (Fig. 4). There is no trend in zonal wind speed over large parts of Dronning Maud Land, with the exception of near Jutulstraumen Glacier where there is a trend for strengthening wind in the westerly direction (Fig. 4). There is large interannual variability in precipitation over Shirase Glacier (Fig. 3c) and no obvious link to observations in ice speed or ice thickness.

229
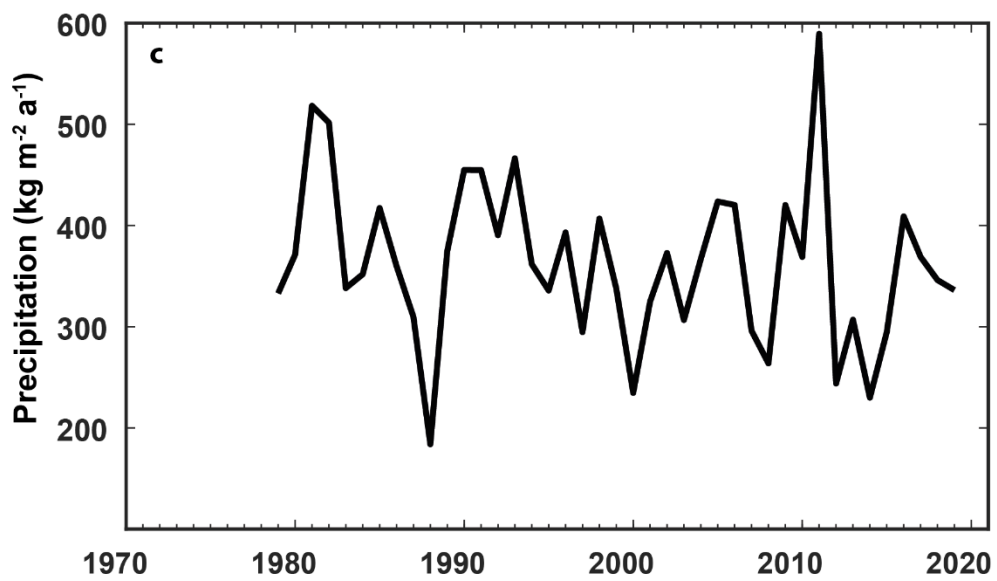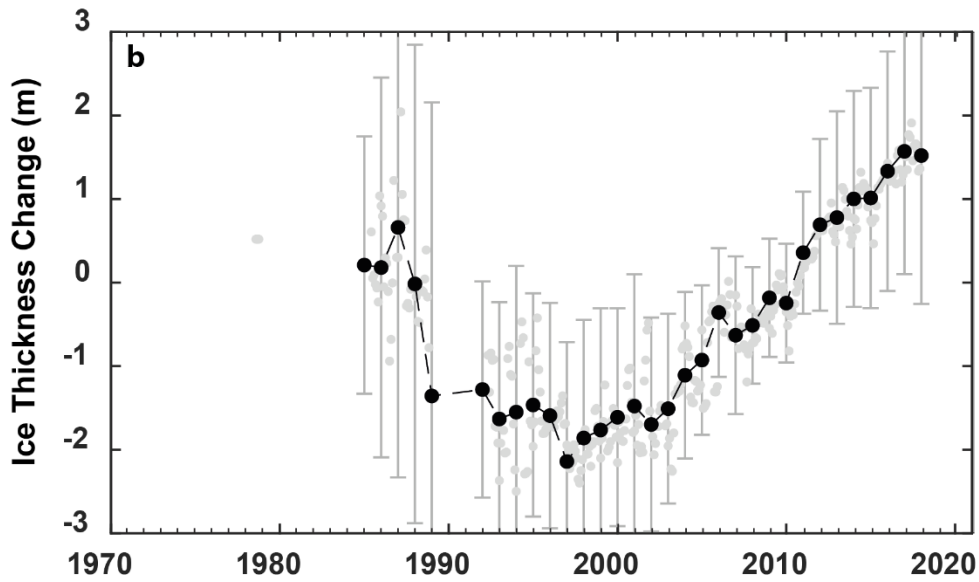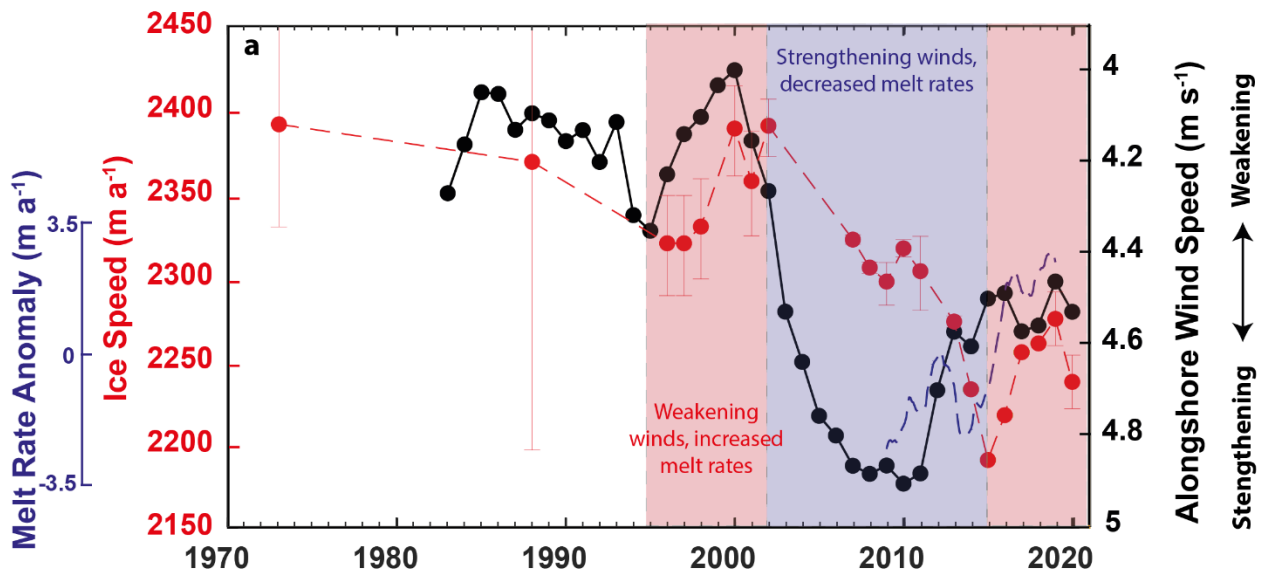
Figure 3: a) Annually averaged ERA5 derived alongshore wind speed from Box A (See Fig. 1) and plotted as a 5-year rolling mean (black), ice speed at the Shirase Glacier grounding line along T1 (red) and modelled melt rate anomaly of the Shirase ice tongue between 2008 and 2018 (blue; Kusahara et al., 2021). Periods of weakening winds cause increased mCDW transport, increased basal melt and acceleration. Periods of strengthening winds result in relatively less mCDW transport, decreased basal melt rates and glacier slowdown. Note that alongshore wind speed is plotted with an inverted axis. **b)** Annually averaged ice thickness change at point IT (see Fig. 2a) extracted from the Schröder et al. (2019) dataset, where there are at least 6 data points in the calendar year. The error bars are annually averaged errors. The background grey points are the raw monthly data points. **c)** Annual averaged precipitation over Shirase Glacier from the MAR regional climate model (Kittel et al., 2021).
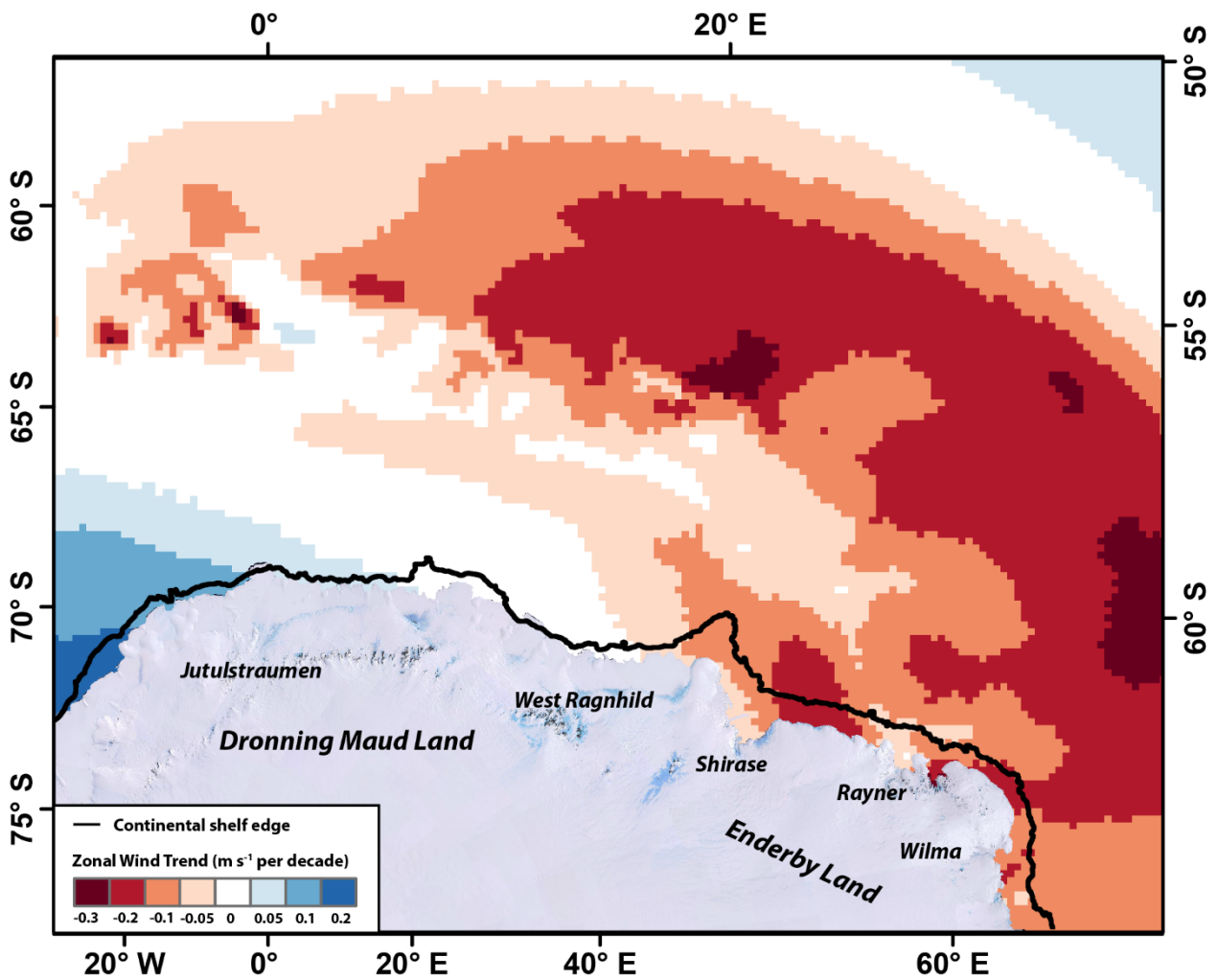
Figure 4: Linear zonal wind trend 1979-2021 with data smoothed with 60 month moving average prior to extracting the trend. Negative values indicate a trend for zonal winds in a more easterly direction and positive values indicate a trend for winds in a more westerly direction. Major outlet glaciers have been labelled.

4. Discussion

4.1 Slowdown and thickening caused by strengthening alongshore winds

Calculations indicate that the heavily fractured and unconstrained section of the Shirase ice tongue offers little buttressing force (Fig. 5a; Durrand et al., 2016; Fürst et al., 2016). Therefore, it is unlikely that any varations in the extent of the Shirase ice tongue have had a direct effect on the ice speed trends we have observed. The only possible exception to this is in 1988 where the ice tongue briefly retreated to the edge of its more confined embayment (Fig. 2a), closer to where the extent of the ice tongue might be expected to exert buttressing and impact on inland flow speed, were it to be removed (Fig. 5a).
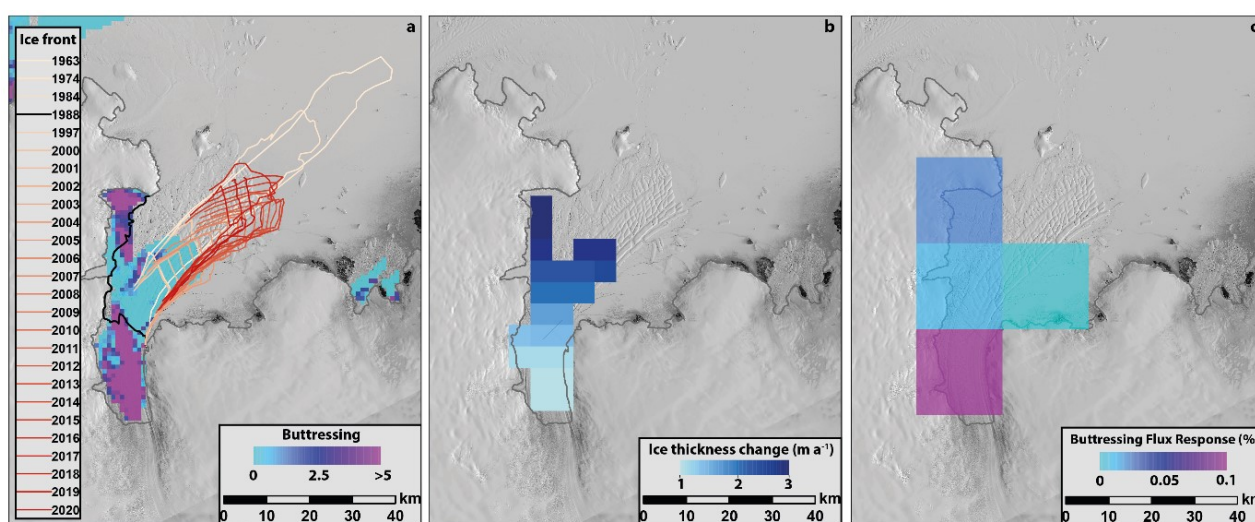
Figure 5: a) Simulated maximum buttressing potential of the Shirase ice tongue (Durand et al., 2016). Light blues mean the ice is passive, purples mean the floating ice is dynamically important. Note how the ice tongue conglomerate is not important for buttressing, but parts of the inner shelf are important. No dynamically important ice has calved over the past over the past 57 years. **b)** Ice tongue thickness change between 2003 and 2019 showing thickening of the Shirase ice tongue (Smith et al., 2020). **c)** Simulated response of ice flux to thinning of floating ice in each grid cell by 1 m (Reese et al., 2018), the constrained inner tongue near the grounding line is important for buttressing. Note there is no change in ice tongue buttressing in response to observed changes in ice tongue extent, but increased buttressing expected in response to observed ice tongue thickening. Landsat images are courtesy of the U.S. Geological Survey.

In agreement with previous work, we note that the observed fluctuations in ice tongue extent are correlated with landfast sea-ice conditions in Lützow-Holm Bay (Aoki, 2017). Long periods of ice tongue advance are associated with persistent landfast sea-ice in Lützow-Holm Bay, while ice tongue retreat is associated with landfast sea-ice break-out events removing parts of the ice tongue conglomerate (Aoki et al., 2017). While there are some sporadic partial break-outs in the landfast sea-

ice during the austral summer months (Fig. S1), there is no evidence of any major changes in fast ice coverage over the course of our observational time period. It is important to note that fast ice only helps control the length of the ice tongue conglomerate (Fig. 1b) and it is unlikely that the fast ice has any major role in providing buttressing for Shirase Glacier. For example, we note that there was no obvious increase in ice speed at the grounding line or over the ice tongue in 1988 when the fast ice and ice tongue conglomerate were completely removed from the bay (Fig. 2a, S3). In addition, Nakamura et al. (2010) recorded only a very modest 20 ± 30 m a^{-1} (0.8 ± 1.3 %) change in ice speed at the grounding line after a partial fast ice break-out event in 1998.

Point IT, 20 km inland of the Shirase Glacier grounding line was thinning at a rate of -0.27 ± 0.33 m a^{-1} between 1987 and 1997 (Fig. 3c), a pattern consistent with field observations up to 200 km further inland in the 1960s, 1970s and 1980s (Mae and Naruse, 1978; Naruse, 1979; Nisho et al., 1989; Toh and Shibuya, 1992). However, in ~2000 there was a slowdown in Shirase Glacier (Fig. 3a) and this thinning trend reversed to thickening (Fig. 3b). This slowdown and thickening coincides with an increase in alongshore wind speed adjacent to the Shirase coastline (Fig. 3a). The seasonal strenghtening in alongshore winds offshore of the Shirase coastline has been observed to deepen the thermocline in Lützow-Holm Bay, limiting the inflow of mCDW onto the continental shelf and reduce basal melt rates (Hirano et al., 2020). We suggest that this same process over annual to decadal timescales has caused the slowdown of Shirase Glacier.

Increased alongshore wind speed from ~2000 enhanced Ekman convergence at the coast, deepening the thermocline with a short lag and inhibited the inflow of warm mCDW into Lützow-Holm Bay. The subsequent cooling of Lützow-Holm Bay reduced the basal melt rate of the Shirase ice tongue. This reduction in basal melt caused the ice tongue to thicken and is confirmed by ICESat and ICESat-2 observations of the of the Shirase ice tongue that show a mean thickening of 1.87 m yr^{-1} from 2003-2019 (Fig. 5b; Smith et al., 2020). Instantaneous numerical modelling experiments show that ice discharge is sensitive to thickness changes in the inner ice tongue (Reese et al., 2018; Fig. 5c). Therefore, the dynamic thickening of the inner ice tongue would be expected to increase buttressing through time (Fig. 5c) and ultimately drive the overall slowdown in ice speed, grounding line advance and inland thickening that we observe. Importantly, our results show that wind-driven ocean forcing is also contributing to mass gain in the Lützow-Holm Bay in addition to surface mass balance processes across the wider region (Boening et al., 2012; Lenaerts et al., 2013).

Within the longer-term slowdown of Shirase Glacier between 1973 and 2020 we observe brief periods of acceleration in response to short-lived periods of weakening alongshore winds. For example, both of the accelerations in ice speed from 1997-2000 and 2015-2019 are preceded by brief periods of weakening alongshore winds (Fig. 3a). These periods of weakening alongshore winds cause relatively

higher basal melt rates because they raise the thermocline closer to the ocean surface and enable a greater influx of mCDW into Lützow-Holm Bay (Hirano et al., 2020). This is supported by the close relationship between alongshore wind speed and modelled melt rate anomalies (Fig. 3a; Kusahara et al., 2021). However, we would not expect a perfect relationship between alongshore wind, melt rates and ice speed particularly over short interannual timescales. For example, an increase in melt rates could cause the ice tongue to thin and accelerate or simply thicken at a lower rate and continue to slowdown.

The interannual variability in ice flow speed at Shirase Glacier in response to wind-forced ocean variability is analogous to other regions of Antarctica where mCDW periodically floods the continental shelf e.g. Pine Island (Christianson et al., 2016), Thwaites (Miles et al., 2020) and Totten glaciers (Greene et al., 2017).The pattern of change at Shirase Glacier is unique, however, in that it is the only outlet glacier in Antarctica with a warm water regime that has been observed to be slowing down and thickening during the 21st century, as opposed to accelerating and thinning (e.g. Mouginot et al., 2014; Greene et al., 2017). As such, our results highlight that this oceanic mode of ice melt is not universally associated with mass loss in Antarctica.

4.2 Wider links to climate forcing and future implications

In response to both increased greenhouse gas emissions and ozone depletion (Thompson et al., 2011; Wang et al., 2014; Perren et al., 2020) the band of mid-latitude westerly winds that encircle Antarctica have both strengthened and migrated southwards towards the ice sheet over recent decades (Thompson & Solomon, 2002; Marshall, 2003; Turner, 2005; Bracegirdle et al., 2018). In the Amundsen Sea sector of West Antarctica, this anthropogenically-driven migration has been linked to westerly wind anomalies over the continental shelf (Holland et al., 2019), which have enabled a greater influx of warm mCDW onto the continental shelf and have driven enhanced localized ice sheet mass loss (Thoma et al., 2008). At Shirase Glacier, our observations of strengthening alongshore easterly winds suggest any southward encroachment of the mid-latitude westerlies has yet to impact the Shirase coastline. This may also be the case for parts of the wider Enderby Land coastlines where alongshore easterlies have also been observed to have strengthened along the continental shelf edge (Hazel & Stewart, 2019). However, it remains unknown what effect these strengthening easterly winds may have had on other nearby outlet glaciers (e.g. Rayner and Wilma; Fig. 4), which are yet to be studied in detail. The trend in strengthening alongshore easterlies might also be linked to enhanced katabatic winds as low pressure systems track progressively further south and enhance the pole to coast pressure gradient (Hazel & Stewart, 2019). It is unclear if the enhancement of the pole-

to-coast pressure gradient has been influenced by the anthropogenically-driven southerly migration of the mid-latitude westerlies, or if it has been caused by inherent natural decadal variability within the system.

Over the course of the 21st century, the southerly migration of the mid-latitude westerlies is projected to continue in a warming climate (Yin, 2005; Perren et al., 2020). Along the Shirase coastline, this continued southerly migration may ultimately result in a similar situation to the Amundsen Sea, such that westerly wind anomalies offshore would result in enhanced mCDW transport into Lützow-Holm Bay and cause mass loss. Alternatively, the westerly winds may never migrate close enough to the Shirase coastline to impact alongshore winds, and instead, alongshore winds may continue to strengthen as the pole to coast pressure gradient increases. This would result in further cooling of Lützow-Holm Bay and ice tongue thickening, and further mass gain. In a wider context, an improved understanding of the potential changes in ocean forcing in response to broader atmospheric patterns expected over the coming decades is needed in the Enderby and Dronning Maud Land sectors.

5. Conclusion

Our observations of Shirase Glacier are a rare example of a glacier reversing a trend of mass loss from at least the 1970s-1990s to mass gain over the last two decades. As far as we are aware this is the only major fast flowing Antarctic outler glacier to display this pattern of behaviour. This reversal has been driven by a slowdown of the Shirase Glacier upstream of the grounding line in response to strengthening alongshore winds that have limited the inflow of warm mCDW into Lützow-Holm Bay, reduced basal melt rates, and caused its ice tongue to dynamically thicken. Should this strengthening of alongshore easterly winds continue into the future, the Shirase catchment will continue to experience a positive mass balance due to both the slow-down in ice discharge, and to the predicted increase in precipitation in response to atmopsheric warming (e.g. Ligtenberg et al., 2013; Kittel et al., 2021). Our results highlight the need for a greater consideration of the potential role of ocean forcing in both the current and future mass balance of the wider Enderby and Dronning Maud Land regions.

Data Availability

Landsat and ARGON imagery was provided free of charge by the US Geological Survey Earth Resources Observation Science Center (https://earthexplorer.usgs.gov/). For the MODIS imagery we also acknowledge the use of imagery from the NASA Worldview application

(https://worldview.earthdata.nasa.gov), part of the NASA Earth Observing System Data and Information System (EOSDIS). Cosi-corr is an ENVI plug-in and can be downloaded from http://www.tectonics.caltech.edu/slip_history/spot_coseis/download_software.html. The ITS_LIVE velocity products are available from https://doi.org/10.5067/IMR9D3PEI28U. GoLIVE velocity products are avaialble from http://dx.doi.org/10.7265/N5ZP442B. ERA5 data is available from https://doi.org/10.24381/cds.adbb2d47. Wind data from Syowa station is available via the SCAR READER at http://dx.doi.org/10.5285/569d53fb-9b90-47a6-b3ca-26306e696706. The MOA grounding line product is avaialble at https://doi.org/10.7265/N5KP8037. BedMachine is available at https://doi.org/10.5067/E1QL9HFQ7A8M. The ice shelf thickness change dataset from Smith et al. (2020) is available at http://hdl.handle.net/1773/45388. REMA DEM strips are avialble at https://www.pgc.umn.edu/data/rema/. Lützow-Holm Bay bathymetry is available at https://doi.org/10.17632/z6w4xd6s3s.1. The RAMP mosaic is available at https://doi.org/10.5067/8AF4ZRPULS4H. Ice shelf extent buttressing dataset from Durand et al., 2016 is available at https://doi.org/10.5067/FWHORAYVZCE7. SPIRIT DEM's are available from https://theia.cnes.fr/atdistrib/rocket/#/search?collection=Spirit. MAR precipitation data is available from https://doi.org/10.5281/zenodo.4459259.

Acknowledgements

This research has been supported by a UK Natural Environment Research Council (NERC) grant (NE/R000824/1). BM was also supported by a Leverhulme Early Career Fellowship (ECF-2021-484). Hersbach, H. et al.'s (2018) dataset was downloaded from the Copernicus Climate Change Service (C3S) Climate Data Store. We acknowledge the DEMs provided by the Byrd Polar and Climate Research Center and the Polar Geospatial Center under NSF-OPP awards 1543501, 1810976, 1542736, 1559691, 1043681, 1541332, 0753663, 1548562, 1238993 and NASA award NNX10AN61G. Computer time provided through a Blue Waters Innovation Initiative. DEMs produced using data from Maxar. We thank Ronja Reese for providing the ice flux buttressing response dataset. We would like to thank two anonymous reviewers, along with the editor Etienne Berthier, for providing constructive comments which led to the improvement of this paper.

Author contributions: All authors contributed to the design of the study. BWJM collected and analysed the remote sensing data and led the manuscript writing with input from all authors.

Competing interests: The authors declare no competing interests

References

Aoki, S., Ozawa, T. & Doi, K. (2000). GPS observation of the sea level variation in Lützow-Holm Bay, Antarctica. *Geophysical Research Letters, 27(15), 2285-2288.* *https://doi.org/10.1029/1999GL011304*

Aoki, S. (2017). Breakup of land-fast sea ice in Lützow-Holm Bay, East Antarctica, and its teleconnection to tropical Pacific sea surface temperatures. *Geophysical Research Letters*, *44*(7), 3219–3227. https://doi.org/10.1002/2017GL072835

Aoyama, Y., Doi, K., Shibuya, K., Ohta, H., & Tsuwa, I. (2013). Near real-time monitoring of flow velocity and direction in the floating ice tongue of the Shirase Glacier using low-cost GPS buoys. *Earth, Planets and Space*, *65*(2), 103–108. https://doi.org/10.5047/EPS.2012.06.011

Boening, C., Lebsock, M., Landerer, F., & Stephens, G. (2012). Snowfall-driven mass change on the East Antarctic ice sheet. *Geophysical Research Letters*, *39*(21). https://doi.org/10.1029/2012GL053316

Bracegirdle, T. J., Hyder, P., & Holmes, C. R. (2018). CMIP5 Diversity in Southern Westerly Jet Projections Related to Historical Sea Ice Area: Strong Link to Strengthening and Weak Link to Shift. *Journal of Climate*, *31*(1), 195–211. https://doi.org/10.1175/JCLI-D-17-0320.1

Brunt, K. M., Fricker, H. A., Padman, L., Scambos, T. A., & O'Neel, S. (2010). Mapping the grounding zone of the Ross Ice Shelf, Antarctica, using ICESat laser altimetry. Annals of Glaciology, 51(55), 71–79. https://doi.org/10.3189/172756410791392790

Christianson, K., Bushuk, M., Dutrieux, P., Parizek, B. R., Joughin, I. R., Alley, R. B., et al. (2016). Sensitivity of Pine Island Glacier to observed ocean forcing. *Geophysical Research Letters*, *43*(20), 10,817-10,825. https://doi.org/10.1002/2016GL070500

Cook, A. J., Holland, P. R., Meredith, M. P., Murray, T., Luckman, A., & Vaughan, D. G. (2016). Ocean forcing of glacier retreat in the western Antarctic Peninsula. *Science*, *353*(6296), 283–286.

Durand, G., F. Gillet-Chaulet, O. Gagliardini, and J. J. Fürst. (2016). SUMER Antarctic Ice-shelf Buttressing, Version 1. Boulder, Colorado USA. NASA National Snow and Ice Data Center Distributed Active Archive Center. https://doi.org/10.5067/FWHORAYVZCE7.

Fahnestock, M., Scambos, T., Moon, T., Gardner, A., Haran, T., & Klinger, M. (2016). Rapid large-area mapping of ice flow using Landsat 8. *Remote Sensing of Environment*, *185*, 84–94. https://doi.org/10.1016/J.RSE.2015.11.023

Fricker, H. A., Coleman, R., Padman, L., Scambos, T. A., Bohlander, J., & Brunt, K. M. (2009). Mapping the grounding zone of the Amery Ice Shelf, East Antarctica using InSAR, MODIS and ICESat. Antarctic Science, 21(5), 515–532. https://doi.org/10.1017/S095410200999023X

Fürst, J. J., Durand, G., Gillet-Chaulet, F., Tavard, L., Rankl, M., Braun, M., & Gagliardini, O. (2016). The safety band of Antarctic ice shelves. *Nature Climate Change*, *6*(5), 479–482. https://doi.org/10.1038/nclimate2912

Gardner, A., Fahnestock, M., & Scambos, T. A. (2020). ITS_LIVE Regional Glacier and Ice Sheet Surface Velocities. https://doi.org/doi:10.5067/6II6VW8LLWJ7

447 Gardner, A. S., Moholdt, G., Scambos, T., Fahnstock, M., Ligtenberg, S., van den Broeke M., &
448   Nilsson, J. (2018). Increased West Antarctic and unchanged East Antarctic ice discharge over
449   the last 7 years. *Cryosphere*, *12*(2), 521–547. https://doi.org/10.5194/TC-12-521-2018

450 Greene, C. A., Blankenship, D. D., Gwyther, D. E., Silvano, A., & van Wijk, E. (2017). Wind
451   causes Totten Ice Shelf melt and acceleration. *Science Advances*, *3*(11), e1701681–e1701681.
452   https://doi.org/10.1126/sciadv.1701681

453 Haran, T., J. Bohlander, T. Scambos, T. Painter, and M. Fahnestock. (2019), updated 2019. MODIS
454   Mosaic of Antarctica 2008-2009 (MOA2009) Image Map, Version 2. Boulder, Colorado USA.
455   NASA National Snow and Ice Data Center Distributed Active Archive Center. doi:
456   https://doi.org/10.5067/4ZL43A4619AF.

457 Hazel, J. E., & Stewart, A. L. (2019). Are the Near-Antarctic Easterly Winds Weakening in
458   Response to Enhancement of the Southern Annular Mode? *Source: Journal of Climate*, *32*(6),
459   1895–1918. https://doi.org/10.2307/26663209

460 Hersbach, H., Bell, B., Berrisford, P., Hirahara, S., Horányi, A., Muñoz-Sabater, J., et al. (2020).
461   The ERA5 global reanalysis. *Quarterly Journal of the Royal Meteorological Society*, *146*(730),
462   1999–2049. https://doi.org/10.1002/QJ.3803

463 Heid, T., & Kääb, A. (2012). Evaluation of existing image matching methods for deriving glacier
464   surface displacements globally from optical satellite imagery. Remote Sensing of
465   Environment, 118, 339–355. https://doi.org/10.1016/J.RSE.2011.11.024

466 Hirano, D., Tamura, T., Kusahara, K., Ohshima, K. I., Nicholls, K. W., Ushio, S., et al. (2020).
467   Strong ice-ocean interaction beneath Shirase Glacier Tongue in East Antarctica. *Nature
468   Communications 2020 11:1*, *11*(1), 1–12. https://doi.org/10.1038/s41467-020-17527-4

469 Holland, P. R., Bracegirdle, T. J., Dutrieux, P., Jenkins, A., & Steig, E. J. (2019). West Antarctic ice
470   loss influenced by internal climate variability and anthropogenic forcing. *Nature Geoscience
471   2019 12:9*, *12*(9), 718–724. https://doi.org/10.1038/s41561-019-0420-9

472 Howat, I. M., Porter, C., Smith, B. E., Noh, M. J., & Morin, P. (2019). The reference elevation
473   model of antarctica. Cryosphere, 13(2), 665–674. https://doi.org/10.5194/TC-13-665-2019

474 Jacobs, S. S., Helmer, H. H., Doake, C. S. M., Jenkins, A., & Frolich, R. M. (1992). Melting of ice
475   shelves and the mass balance of Antarctica. *Journal of Glaciology*, *38*(130), 375–387.
476   https://doi.org/10.3189/S0022143000002252

477 Jenkins, A., Shoosmith, D., Dutrieux, P., Jacobs, S., Kim, T. W., Lee, S. H., et al. (2018). West
478   Antarctic Ice Sheet retreat in the Amundsen Sea driven by decadal oceanic variability, *11*(10),
479   733–738. https://doi.org/10.1038/s41561-018-0207-4

480 Jezek, K. C., J. C. Curlander, F. Carsey, C. Wales, and R. G. Barry. (2013). RAMP AMM-1 SAR
481   Image Mosaic of Antarctica, Version 2. Boulder, Colorado USA. NASA National Snow and
482   Ice Data Center Distributed Active Archive Center. https://doi.org/10.5067/8AF4ZRPULS4H.

483 Kameda, T., Nakawo, M., Mae, S., Watanabe, O., & Naruse, R. (1990). Thinning of the Ice Sheet
484   Estimated from Total Gas Content of Ice Cores in Mizuho Plateau, East Antarctica. *Annals of
485   Glaciology*, *14*, 131–135. https://doi.org/10.3189/S0260305500008429

486 Kittel, C., Amory, C., Agosta, C., Jourdain, N. C., Hofer, S., Delhasse, A., et al. (2021). Diverging
487   future surface mass balance between the Antarctic ice shelves and grounded ice sheet.
488   *Cryosphere*, *15*(3), 1215–1236. https://doi.org/10.5194/TC-15-1215-2021

489 Konrad, H., Shepherd, A., Gilbert, L., Hogg, A. E., McMillan, M., Muir, A., & Slater, T. (2018).
490   Net retreat of Antarctic glacier grounding lines. Nature Geoscience, 11(4), 258–262.
491   https://doi.org/10.1038/s41561-018-0082-z

492 Korona, J, Berthier, E, Bernard, M, Rémy, F and Thouvenot, E (2009) ISPRS Journal of
493   Photogrammetry and Remote Sensing SPIRIT. SPOT 5 stereoscopic survey of Polar Ice:
494   reference images and topographies during the fourth International Polar Year (2007–2009).
495   ISPRS Journal of Photogrammetry and Remote Sensing 64(2), 204–212. doi:
496   10.1016/j.isprsjprs.2008.10.005.

497 Kusahara, K., Hirano, D., Fujii, M., D. Fraser, A., & Tamura, T. (2021). Modeling intensive ocean-
498   cryosphere interactions in Lützow-Holm Bay, East Antarctica. *Cryosphere*, *15*(4), 1697–1717.
499   https://doi.org/10.5194/TC-15-1697-2021

500 Lenaerts, J. T. M., van Meijgaard, E., van den Broeke, M. R., Ligtenberg, S. R. M., Horwath, M., &
501   Isaksson, E. (2013). Recent snowfall anomalies in Dronning Maud Land, East Antarctica, in a
502   historical and future climate perspective. *Geophysical Research Letters*, *40*(11), 2684–2688.
503   https://doi.org/10.1002/GRL.50559

504 Leprince, S., Ayoub, F., Klinger, Y., & Avouac, J.-P. (2007). *Co-Registration of Optically Sensed*
505   *Images and Correlation (COSI-Corr): an Operational Methodology for Ground Deformation*
506   *Measurements*. Igarss: 2007 Ieee International Geoscience and Remote Sensing Symposium,
507   1–12,1943–1946. https://doi.org/10.1109/Igarss.2007.4423207

508 Ligtenberg, S. R. M., van de Berg, W. J., van den Broeke, M. R., Rae, J. G. L., & van Meijgaard, E.
509   (2013). Future surface mass balance of the Antarctic ice sheet and its influence on sea level
510   change, simulated by a regional atmospheric climate model. *Climate Dynamics*, *41*(3–4), 867–
511   884. https://doi.org/10.1007/S00382-013-1749-1

512 Mae, S., & Naruse, R. (1978). Possible causes of ice sheet thinning in the Mizuho Plateau. *Nature*
513   *1978 273:5660*, *273*(5660), 291–292. https://doi.org/10.1038/273291a0

514 Marshall, G. (2003). Trends in the Southern Annular Mode from observations and reanalyses. *J.*
515   *Clim.*, *16*, 4134–4143.

516 Miles, B. W. J. J., Stokes, C. R., Jenkins, A., Jordan, J. R., Jamieson, S. S. R. R., & Gudmundsson,
517   G. H. (2020). Intermittent structural weakening and acceleration of the Thwaites Glacier
518   Tongue between 2000 and 2018. *Journal of Glaciology*, 1–11.
519   https://doi.org/10.1017/jog.2020.20

520 Moriwaki, K., & Yoshida, Y. (1983). Submarine topography of Lützow-Holm Bay, Antarctica.
521   *Mem. Natl. Inst. Polar Res.*, *28*, 247–258.

522 Morlighem, M. (2020). MEaSUREs BedMachine Antarctica, Version 2. Boulder, Colorado USA.
523   NASA National Snow and Ice Data Center Distributed Active Archive Center. doi:
524   https://doi.org/10.5067/E1QL9HFQ7A8M.

525 Morlighem, M., Rignot, E., Binder, T., Blankenship, D., Drews, R., Eagles, G., et al. (2020). Deep
526   glacial troughs and stabilizing ridges unveiled beneath the margins of the Antarctic ice sheet.
527   *Nature Geoscience*, *13*(2), 132–137. https://doi.org/10.1038/s41561-019-0510-8

Mouginot, J., Rignot, E., & Scheuchl, B. (2014). Sustained increase in ice discharge from the Amundsen Sea Embayment, West Antarctica, from 1973 to 2013. *Geophysical Research Letters*, *41*(5), 1576–1584. https://doi.org/10.1002/2013GL059069

Nakamura, K., Doi, K., & Shibuya, K. (2007). Estimation of seasonal changes in the flow of Shirase Glacier using JERS-1/SAR image correlation. *Polar Science*, *1*(2–4), 73–83. https://doi.org/10.1016/J.POLAR.2007.09.002

Nakamura, K., Doi, K., & Shibuya, K. (2010). Fluctuations in the flow velocity of the Antarctic Shirase Glacier over an 11-year period. *Polar Science*, *4*(3), 443–455. https://doi.org/10.1016/J.POLAR.2010.04.010

Naruse, R. (1979). Thinning of the Ice Sheet in Mizuho Plateau, East Antarctica. *Journal of Glaciology*, *24*(90), 45–52. https://doi.org/10.3189/S0022143000014635

Nishio, F., Mae, S., Ohmae, H., Takahashi, S., Nakawo, M., & Kawada, K. (1989). Dynamical behaviour of the ice sheet in Mizuho Plateau, East Antarctica. *Proc. NIPR Symp. Polar Meteorol. Glaciol.*, *2*, 97–104.

Ohshima, K. I., Takizawa, T., Ushio, S., & Kawamura, T. (1996). Seasonal variations of the Antarctic coastal ocean in the vicinity of Lützow-Holm Bay. *Journal of Geophysical Research C: Oceans*, *101*(C9), 20617–20628. https://doi.org/10.1029/96JC01752

Pattyn, F., & Derauw, D. (2002). Ice-dynamic conditions of Shirase Glacier, Antarctica, inferred from ERS SAR interferometry. *Journal of Glaciology*, *48*(163), 559–565. https://doi.org/10.3189/172756502781831115

Pattyn, F., & Naruse, R. (2003). The nature of complex ice flow in Shirase Glacier catchment, East Antarctica. *Journal of Glaciology*, *49*(166), 429–436. https://doi.org/10.3189/172756503781830610

Perren, B. B., Hodgson, D. A., Roberts, S. J., Sime, L., van Nieuwenhuyze, W., Verleyen, E., & Vyverman, W. (2020). Southward migration of the Southern Hemisphere westerly winds corresponds with warming climate over centennial timescales. *Communications Earth & Environment 2020 1:1*, *1*(1), 1–8. https://doi.org/10.1038/s43247-020-00059-6

Reese, R., Gudmundsson, G. H., Levermann, A., & Winkelmann, R. (2018). The far reach of ice-shelf thinning in Antarctica. Nature Climate Change, 8(1), 53– 57. https://doi.org/10.1038/s41558-017-0020-x

Rignot, E., Mouginot, J., Scheuchl, B., van den Broeke, M., van Wessem, M. J., & Morlighem, M. (2019, January 22). Four decades of Antarctic ice sheet mass balance from 1979–2017. *Proceedings of the National Academy of Sciences of the United States of America*. National Academy of Sciences. https://doi.org/10.1073/pnas.1812883116

Rintoul, S. R., Silvano, A., Pena-Molino, B., van Wijk, E., Rosenberg, M., Greenbaum, J. S., & Blankenship, D. D. (2016). Ocean heat drives rapid basal melt of the Totten ice shelf. *Science Advances*, *2*(12). https://doi.org/10.1126/sciadv.1601610

Scambos, T., Fahnestock, M., Moon, T., Gardner, A., & Klinger, M. (2016). Global Land Ice Velocity Extraction from Landsat 8 (GoLIVE). Boulder, Colorado USA. NSIDC: National Snow and Ice Data Center.

Scambos, T. A., Haran, T. M., Fahnestock, M. A., Painter, T. H., & Bohlander, J. (2007). MODIS-based Mosaic of Antarctica (MOA) data sets: Continent-wide surface morphology and snow grain size. *Remote Sensing of Environment*, *111*(2), 242–257. https://doi.org/10.1016/J.RSE.2006.12.020

Scherler, D., Leprince, S., & Strecker, M. R. (2008). Glacier-surface velocities in alpine terrain from optical satellite imagery—Accuracy improvement and quality assessment. *Remote Sensing of Environment*, *112*(10), 3806–3819. https://doi.org/10.1016/J.RSE.2008.05.018

Schröder, L., Horwath, M., Dietrich, R., & Helm, V. (2019). Four decades of surface elevation change of the Antarctic Ice Sheet from multi-mission satellite altimetry. *The Cryosphere*, 13, 427–449, https://doi.org/10.5194/tc-13-427-2019

Smith, B., Fricker, H. A., Gardner, A. S., Medley, B., Nilsson, J., Paolo, F. S., Nicholas Holschuh, et al. (2020). Pervasive ice sheet mass loss reflects competing ocean and atmosphere processes. *Science*, *368*(6496), 1239–1242.

Sproson, A. D., Takano, Y., Miyairi, Y., Aze, T., Matsuzaki, H., Ohkouchi, N., & Yokoyama, Y. (2021). Beryllium isotopes in sediments from Lake Maruwan Oike and Lake Skallen, East Antarctica, reveal substantial glacial discharge during the late Holocene. *Quaternary Science Reviews*, *256*, 106841. https://doi.org/10.1016/J.QUASCIREV.2021.106841

Stokes, C.R., Abram, N.J., Bentley, M.J. et al. Response of the East Antarctic Ice Sheet to past and future climate change. Nature 608, 275–286 (2022). https://doi.org/10.1038/s41586-022-04946-0

Thoma, M., Jenkins, A., Holland, D., & Jacobs, S. (2008). Modelling Circumpolar Deep Water intrusions on the Amundsen Sea continental shelf, Antarctica. *Geophysical Research Letters*, *35*(18). https://doi.org/10.1029/2008GL034939

Thompson, D. W. J., & Solomon, S. (2002). Interpretation of recent Southern Hemisphere climate change. *Science*, *296*(5569), 895–899. https://doi.org/10.1126/science.1069270

Thompson, D. W. J., Solomon, S., Kushner, P. J., England, M. H., Grise, K. M., & Karoly, D. J. (2011). Signatures of the Antarctic ozone hole in Southern Hemisphere surface climate change. *Nature Geoscience 2011 4:11*, *4*(11), 741–749. https://doi.org/10.1038/ngeo1296

Toh, H. and Shibuya, K. (1992). Thinning rate of ice sheet on Mizuho Plateau, East Antarctica, determined by GPS differential positioning. In Yoshida, Y., Kaminuma, K. and Shiraishi, K., eds. Recent progress in Antarctic earth sciences. Tokyo, Terra Scientific Publishing Co., 579–583.

Turner, J., Colwell, S. R., Marshall, G. J., Lachlan-Cope, T. A., Carleton, A. M., Jones, P. D., Lagun, V., Reid, P. A., & Iagovkina, S. (2004). The SCAR READER Project: Toward a High-Quality Database of Mean Antarctic Meteorological Observations, Journal of Climate, 17(14), 2890-2898.

Turner, J. (2005). Antarctic climate change during the last 50 years. *Int. J. Climatol.*, *25*, 279–294.

Wang, G., Cai, W., & Purich, A. (2014). Trends in Southern Hemisphere wind-driven circulation in CMIP5 models over the 21st century: Ozone recovery versus greenhouse forcing. *Journal of Geophysical Research: Oceans*, *119*(5), 2974–2986. https://doi.org/10.1002/2013JC009589

608   Yin, J. H. (2005). A consistent poleward shift of the storm tracks in simulations of 21st century
609   climate. *Geophys. Res. Lett.*, *32*(18), L18701. https://doi.org/10.1029/2005gl023684

610